Available online at www.sciencedirect.com
SCIENCE DIRECT®
Chemical Physics 324 (2006) 298–306
Chemical Physics
www.elsevier.com/locate/chemphys

A theoretical investigation for the reaction of CH_3CH_2SH with atomic H: Mechanism and kinetics properties

Qingzhu Zhang *, Haining Wang, Tingli Sun, Wenxing Wang

Environment Research Institute, Shandong University, Jinan 250100, PR China

Received 1 September 2005; accepted 21 October 2005
Available online 13 December 2005

Abstract

The multiple-channel reaction of CH_3CH_2SH with atomic H has been investigated theoretically using ab initio molecular orbital theory for the first time. The profile of the potential energy surface was constructed at the QCISD(T)/6-311 + G(3df, 2p)//MP2/6-311G(2d, p) level. Two kinds of channels have been identified: abstraction and substitution. Abstraction involved in three channels: H abstraction from CH_3 group, H abstraction from CH_2 group, and H abstraction from SH group. The substitution channel will lead to the products of CH_3CH_2 and H_2S. On the basis of ab initio calculation, the rate constants have been deduced using canonical variational transition-state theory with small curvature tunneling contribution over a wide temperature range (200–3000 K). The kinetics properties along the reaction path for each channel have been analyzed and compared. The calculated total rate constants match the available experimental values reasonably well over the measured temperature range. The results show that, the channel of H abstraction from SH group dominant this reaction, while substitution channel will be a strong competitive reaction as the temperature increases.

Keywords: CH_3CH_2SH; H; Multiple-channel reaction mechanism; Direct dynamics; Rate constants; Branching ratios

1. Introduction

Gas phase sulfur compounds represent only a small fraction of the Earth's atmospheric composition, comprising less that 1 ppm by volume in air [1]. However, the chemistry of sulfur compounds has a significant impact on the atmosphere and the biosphere: acid rain, visibility reduction and climate modification. The abundant sulfur-based gases in the atmosphere involve in hydrogen sulfide (H_2S), dimethyl sulfide (CH_3SCH_3), carbon disulfide (CS_2), carbonyl sulfide (OCS), sulfide dioxide (SO_2) and ethanethiol (CH_3CH_2SH), etc. The atmospheric sulfur compounds have a variety of natural and anthropogenic sources [1–4]. The total anthropogenic source strength is roughly two or three times larger than total natural emissions. Most of gas phase sulfur compounds emitted from natural and anthropogenic sources are reductive. These reductive sulfur compounds are oxidized by variety of atmosphere species. The ultimate fate of these atmospheric sulfide compounds is the irreversible oxidation of sulfate (SO_4^{2-}), the sulfur constituent of tropospheric and stratospheric sulfate aerosols (i.e., H_2SO_4, NH_4HSO_4, $(NH_4)_2SO_4$). Recognition of the important of sulfur compounds has led to a substantial research effort to understand its atmospheric chemistry. The modeling of oxidation of sulfur compounds represents important steps of the control of both the production and the elimination of sulfur-containing pollutants. Fundamental knowledge of specific pathways, stable end products, kinetic parameters is vital in evaluating the role of sulfur-containing pollutants in climate regulation and in understanding the biogeochemical cycling of sulfur. In this paper, we have initiated an exhaustive theoretical study of the application of electronic calculations for the microcosmic mechanism and kinetics properties for the reaction of CH_3CH_2SH with H radicals. The largest source of CH_3CH_2SH is the oceanic

* Corresponding author. Fax: +86 531 8836 4435.
E-mail address: zqz@sdu.edu.cn (Q. Zhang).

0301-0104/$ - see front matter © 2005 Elsevier B.V. All rights reserved.
doi:10.1016/j.chemphys.2005.10.040

emission by marine phytoplankton. CH_3CH_2SH is also one of industrial organosulfur pollutants emitted to the atmosphere, for example, the industrial waste gases from the refinery. New applications of CH_3CH_2SH have arisen in recent years, such as its use as a stabilizing agent applying in the bonder, and as a gas giving an alarm. The reaction with atomic H, the simplest free-radical species, is particular interest since this kind of reaction provides an uncomplicated probe of chemical reactivity.

Experimentally, three reports are on record [5–7]. An early paper [5] studied the thermal rate constants for the reaction of CH_3CH_2SH with atomic H. The measured relative rate constant is 1.9 compared with the reaction of C_2H_4 with H at 298 K. In 1988, Martin and his coworkers [6] reported the absolute rate constant measured directly by electron beam and mass spectrometry. The value is $(2.41 \pm 0.16) \times 10^{-12}$ cm^3 molecule^{-1} s^{-1}. In 1989, Lam [7] studied this reaction by direct photolysis and Vis–UV absorption analytical technique. Two channels were revealed: $H + CH_3CH_2SH \rightarrow CH_3CH_2S + H_2$, and $H + CH_3CH_2SH \rightarrow CH_3CH_2 + H_2S$. Arrhenius expressions for the hydrogen atom abstraction and SH-displacement reactions were determined over the temperature range of 298–423 K: $k = (6.64 \pm 1.13) \times 10^{-12} \exp(-1.07 \pm 0.04$ kcal/mol$)/RT$ cm^3 molecule^{-1} s^{-1}, and $k = (8.49 \pm 1.53) \times 10^{-12} \exp(-2.38 \pm 0.07$ kcal/mol$)/RT$ cm^3 molecule^{-1} s^{-1}. The branching ratio is 6.97 ± 0.38 at the temperature of 298 K. To our best knowledge, little theoretical attention has been paid to the reaction of CH_3CH_2SH with atomic H. In the current study, a more detailed microcosmic mechanism was revealed using high level ab initio electronic theory. The kinetics properties for the reaction of CH_3CH_2SH with atomic H have been deduced using interpolated canonical variational transition-state (CVT) theory [8–11] and the centrifugal-dominant, small-curvature tunneling approximation (SCT) [12], including the information at the reactants, products, saddle point, and extra points along the minimum energy path. The calculated results were compared with the measured experimental values.

2. Computational methods

All the electronic structure calculations were carried out with Gaussian 03 program [13] for the reaction of CH_3CH_2SH with atomic H. Full geometry optimizations were performed for reactants, products and saddle points at the unrestricted second-order perturbation Moller–Plesset level of theory (MP2) using the standard 6-311G(2d, p) basis set. Force constant matrixes and related normal mode harmonic vibrational frequencies were calculated at the same level for each stationary point in order to determine the nature of the stationary points, the zero-point energy (ZPE), and the thermal contributions to the free energy of activation. Each saddle point was verified to connect the designated reactants and products by performing an intrinsic reaction coordinate (IRC) [14] analysis. At the MP2/6-311G(2d, p) level, the minimum energy paths (MEP) were constructed in order to carry out the direct dynamics calculations for all channels independently, starting from the saddle point geometry and going downhill to both the asymptotic reactant and product channel with a gradient step size of 0.02 amu$^{1/2}$ bohr. Although the geometrical parameters and the frequencies of various species can be determined satisfactorily at the MP2/6-311G(2d, p) level, the energies obtained at this level may not be accurate enough for the subsequent kinetics calculation. Therefore, a higher level, QCISD(T), and a more flexible basis set, 6-311+G(3df, 2p), were employed to calculate the single-point energies of various species.

By means of Polyrate 9.3 program [15], direct dynamics calculations were carried out using the canonical variational transition-state theory (CVT) for all the channels involved in the reaction of CH_3CH_2SH with atomic H. Canonical variational transition-state theory [8–11] is based on the idea of varying the dividing surface along a reference path to minimize the rate constant. The canonical variational theory (CVT) rate constant for temperature T is given:

$$k^{\mathrm{CVT}}(T) = \min_s k^{\mathrm{GT}}(T, s), \tag{1}$$

where

$$k^{\mathrm{GT}}(T, s) = \frac{\sigma k_{\mathrm{B}} T}{h} \frac{Q^{\mathrm{GT}}(T, s)}{\Phi^{\mathrm{R}}(T)} \mathrm{e}^{-V_{\mathrm{MEP}}(s)/k_{\mathrm{B}}T}, \tag{2}$$

where, $k^{\mathrm{GT}}(T,s)$ is the generalized transition-state theory rate constant at the dividing surface s, σ is the symmetry factor accounting for the possibility of more than one symmetry-related reaction path, k_{B} is Boltzmann's constant, h is Planck's constant, $\Phi^{\mathrm{R}}(T)$ is the reactant partition function per unit volume, excluding symmetry numbers for rotation, and $Q^{\mathrm{GT}}(T,s)$ is the partition function of a generalized transition state at s with a local zero of energy at $V_{\mathrm{MEP}}(s)$ and with all rotational symmetry numbers set to unity. The level of tunneling calculation is the small curvature tunneling (SCT) method, based on the centrifugal-dominant small-curvature semiclassical adiabatic ground-state approximation [12]. Since the heavy–light–heavy mass combination is not present in the title reaction, the SCT theory is regarded to be enough. The rotational partition functions were calculated classically, and the vibrational modes were treated as quantum-mechanical separable harmonic oscillators.

3. Results and discussion

The optimized geometries of the reactant, saddle points, and products along with the experimental values are shown in Figs. 1 and 2. The vibrational frequencies of the reactant, products, and saddle points are listed in Tables 1 and 2. The potential barriers ΔE and the reaction enthalpies ΔH calculated at the QCISD(T)/6-311+G(3df, 2p) level are summarized in Table 3. Fig. 3(a) and (b) shows the classical potential energy (V_{MEP}), zero-point energy

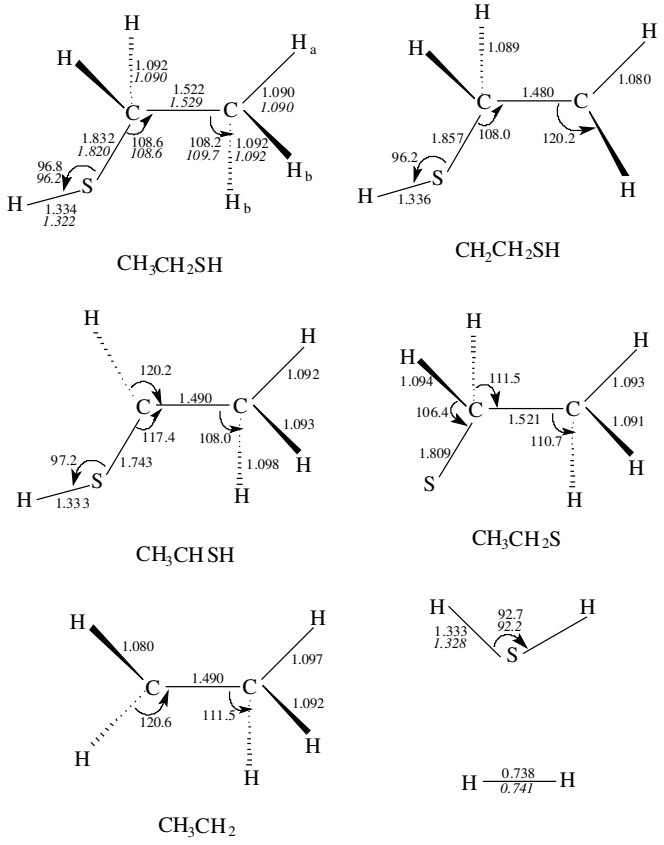

Fig. 1. MP2/6-311G(2d, p) optimized geometries for the reactants and the products. Distances are in angstroms, and angles are in degrees. The values in italic are the experimental data [16,17].

(ZPE) and vibrationally adiabatic potential energy (V_a^G) curves as functions of distance along the reaction coordinate s at the QCISD(T)/6-311+G(3df, 2p)//MP2/6-311G(2d, p) level for the channel of H abstraction from SH group and substitution channel. Changes of the generalized normal-mode vibrational frequencies as functions of the reaction coordinate s are listed in Fig. 4(a) and (b) for the channel of H abstraction from SH group and substitution channel. The CVT/SCT rate constants for each channel and the total rate constants along with the available experimental values are summarized in Table 4 and Fig. 5. The branching ratios are shown in Fig. 6. Fig. 7 shows the calculated TST, CVT, and CVT/SCT rate constants for the channel of H abstraction from CH_2 group.

3.1. Reaction mechanism

Firstly, the expectation values of $\langle S^2 \rangle$ were monitored in the MP2/6-311G(2d, p) optimization. The values of $\langle S^2 \rangle$ are always in the range of 0.750–0.800 for doublets. After spin annihilation, the values of $\langle S^2 \rangle$ are 0.750, where 0.750 is the exact value for a pure doublet. Thus, spin contamination is not severe. This suggests that a single determinant reference wave function for this title system is suitable for the level of theory used in the optimization. It is worth stating the reliability of the calculations in this work. As shown in Fig. 1, the calculated geometric parameters of CH_3CH_2SH, H_2S and H_2 are in excellent agreement with the available experimental values, with the maximum deviation of the bond lengths within 1.0%. As shown in Table 1, the calculated vibrational frequencies of CH_3CH_2SH, CH_3CH_2, H_2S and H_2 agree well with the experimentally observed fundamentals, and the relative error is less than 8.0%. From these comparisons, it might be inferred that the same accuracy could be expected for other species. These good agreements give us confidence that the MP2/6-311G(2d, p) level is adequate to optimize the geometries and calculate the frequencies. For a further comparison, in addition to the MP2/6-311G(2d, p) method, the geometric parameters of the saddle points were also computed at the BB1K/6-311G(2d, p) levels of theory. As shown in Fig. 2, the geometric parameters obtained at two levels match well.

For the reaction of CH_3CH_2SH with atomic H, four primary processes have been identified:

$$CH_3CH_2SH + H \rightarrow CH_2CH_2SH + H_2$$
H abstraction from CH_3 R_1

$$CH_3CH_2SH + H \rightarrow CH_3CHSH + H_2$$
H abstraction fromCH_2 R_2

$$CH_3CH_2SH + H \rightarrow CH_3CH_2S + H_2$$
H abstraction from SH R_3

$$CH_3CH_2SH + H \rightarrow CH_3CH_2 + H_2S$$
substitution channel R_4

Reactant CH_3CH_2SH has C_s symmetry. Three hydrogen atoms in CH_3 group are unequivalent. The H atom (denoted as H_a) in the symmetry plane is different from other atoms (denoted as H_b). In the reactant CH_3CH_2SH structure, the C–H_b bond (1.092 Å) is 0.002 Å longer than the C–H_a bond (1.090 Å). As a result, two channels have been revealed for the hydrogen abstraction from CH_3 group: H abstraction from the C–H_a bond, and H abstraction the C–H_b bond. Therefore, two saddle points were located. The saddle point of H abstraction from the C–H_a bond was denoted as TS_{1a}, and the saddle point of H abstraction from C–H_b bond was denoted as TS_{1b}, whose geometrical parameters were shown in Fig. 2. Saddle points TS_{1a} has C_s symmetry, and TS_{1b} is C_1 symmetry-structure. In the saddle points TS_{1a} and TS_{1b} structures, the breaking C–H bonds increase by 27% with respect to the C–H equilibrium bond length of CH_3CH_2SH, and the forming H–H bonds are 20% longer than the equilibrium bond length of H_2. This result indicates that the barriers of hydrogen abstraction from CH_3 group are almost centrally located, as expected for a weakly exothermic or endothermic reaction (see Table 3). The saddle points of TS_{1a} and TS_{1b} were identified with one negative eigenvalue of the Hessian matrix and, therefore, one imaginary frequency. The large values of the imaginary frequency will narrow the width of the potential barrier. By the conventional VTST, it is known that a narrow barrier is favored tunneling effect.

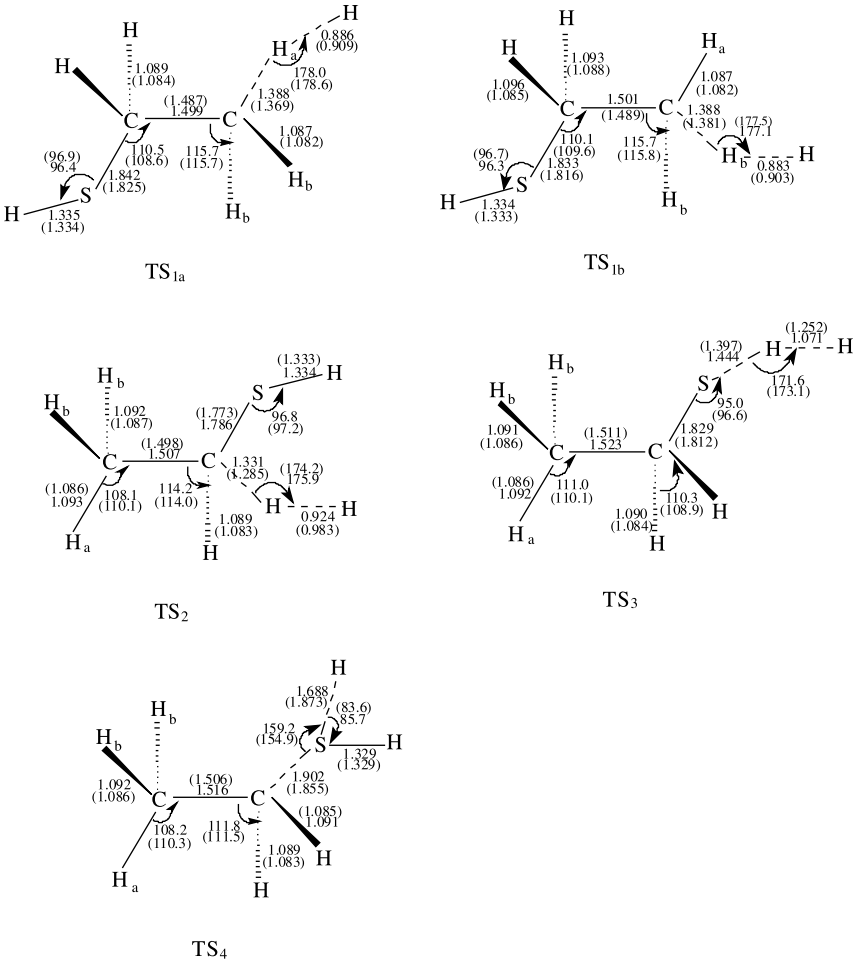

Fig. 2. MP2/6-311G(2d, p) optimized geometries for the saddle points. Distances are in angstrom, and angles are in degree. The values in parentheses are the results obtained at the BB1K/6-311G(2d, p) level.

Table 1
Vibrational frequencies (in cm^{-1}) along with the available experiment values [18–20] for the reactant and products involved in the reaction of CH_3CH_2SH with atomic H at the MP2/6-311G(2d, p) level

Species	Frequencies
CH_3CH_2SH	3172 3160 3151 3103 3074 2778 1533 1525 1516 1437 1318 1287 1125 1065 1012 870 802 689 307 264 176 *2966 2966 2930 2872 2872 2580 1453 1453 1453 1385 1309 1269 1097 1049 978 870 745 660 332*
CH_2CH_2SH	3317 3201 3170 3107 2762 1524 1500 1280 1270 1102 1051 883 796 687 547 286 219 127
CH_3CHSH	3240 3152 3108 3030 2784 1519 1507 1438 1328 1155 1056 1023 906 737 469 308 225 147
CH_3CH_2S	3171 3154 3093 3071 3067 1526 1519 1459 1437 1301 1276 1092 995 910 680 425 333 240
CH_3CH_2	3310 3200 3154 3110 3031 1521 1520 1507 1433 1214 1076 1003 822 456 148 *3033 3112 2987 2842 1440 1440 1375 1366 1138*
H_2S	2805 2786 1233 *2615 2626 1183*
H_2	4534 *4401*

The imaginary frequencies of TS_{1a} and TS_{1b} calculated at the MP2/6-311G(2d, p) level are 1689i and 1673i, respectively. Thus, a significant tunneling contribution might be found in the calculation of the rate constant for the H abstraction from CH_3 group.

For the channel of H abstraction from CH_2 group, a saddle point, denoted as TS_2, was found. At the MP2/6-311G(2d, p) level, the breaking C–H bond in TS_2 stretches by 22% compared with the C–H equilibrium bond length of CH_3CH_2SH, and the forming H–H bond is 25% longer

Table 2
Vibrational frequencies (in cm^{-1}) for the saddle points involved in the reaction of CH_3CH_2SH with atomic H at the MP2/6-311G(2d, p) level

Species	Frequencies
TS_{1a}	3232 3165 3138 3104 2765 1858 1515 1497 1294 1290 1191 1190 1097 1061 990 872 806 707 575 339 237 164 133 1689i
TS_{1b}	3229 3141 3134 3079 2780 1885 1502 1485 1319 1222 1191 1183 1104 1029 1010 886 816 691 564 345 263 197 114 1673i
TS_2	3163 3151 3143 3065 2777 1651 1522 1515 1434 1312 1294 1227 1132 1056 1033 891 858 709 352 315 308 237 200 1799i
TS_3	3171 3158 3151 3100 3073 1532 1524 1514 1435 1396 1314 1286 1116 1066 1009 952 802 690 594 333 260 232 75 1699i
TS_4	3176 3154 3152 3099 3070 2806 1529 1524 1501 1434 1273 1263 1153 1035 1007 989 782 661 585 326 276 241 152 859i

Table 3
The potential barriers ΔE (in kcal/mol) and the reaction enthalpies ΔH (in kcal/mol) calculated at the QCISD(T)/6-311+G(3df, 2p) level for the reaction of CH_3CH_2SH with atomic H

	Energies
ΔE_1	13.3
ΔE_2	13.9
ΔE_3	9.1
ΔE_4	3.2
ΔE_5	3.5
ΔH_1	−0.2
ΔH_2	−0.2
ΔH_3	−8.0
ΔH_4	−18.0
ΔH_5	−16.3

than the equilibrium bond length of H_2. The intrinsic reaction coordinate (IRC) calculation was carried out to verify the transition state TS_2 connects the designated reactants (CH_3CH_2SH and H) and products (CH_3CHSH and H_2). TS_2 was identified with one negative eigenvalue of the Hessian matrix and, therefore, one imaginary frequency of 1799i. Therefore, a larger tunneling effect is expected in the calculation of the rate constant for the H abstraction from CH_2 group. The H abstraction from SH group will proceed via the saddle point TS_3. At the MP2/6-311G(2d, p) level, the breaking C–H bond is elongated by 8% with respect to the S–H equilibrium bond length of CH_3CH_2SH, and the forming H–H bond is 45% longer than the equilibrium bond length of H_2. The saddle point TS_3 is reactant-like. Therefore, the H abstraction channel from SH group will proceed via an early potential barrier. This rather early character in the saddle point TS_3 is in accordance with the low potential barrier and the high exothermicity of this channel (see Table 3), in keeping with Hammond's postulate [21]. The saddle point TS_3 has C_s symmetry. One imaginary frequency of 1699i was found in TS_3.

For the channel of substitution, a saddle point was located, resulting in the products of CH_3CH_2 and H_2S. The saddle point was denoted as TS_4. In the saddle point TS_4 structure, the breaking C–S bond is 4% longer than the equilibrium value in CH_3CH_2SH, while the forming S–H bond is stretched by 27%. Therefore, the substitution channel will proceed via an early potential barrier. TS_4 has one and only one imaginary frequency. For the substitution reaction, another channel leading to the formation of CH_3CH_3 and SH radicals was also studied. At the MP2/6-311G(2d, p) level, a saddle point was found. At the QCISD(T)/6-311 + G(3df, 2p) level, the potential barrier of this channel is 39.4 kcal/mol, which is 35.9 kcal/mol higher than that of the substitution channel resulting in the products of CH_3CH_2 and H_2S. Therefore, the contribution from this channel can be safely neglected, and the kinetics properties of the substitution channel leading to the formation of CH_3CH_3 and SH was not studied in this work.

The single-point energy calculations were carried out at the QCISD(T)/6-311 + G(3df, 2p) level. The obtained potential barriers and the reaction enthalpies are shown in Table 3. First, we analyze the reaction enthalpy. We obtained an experimental reaction enthalpy of −17.2 kcal/mol from the measured $\Delta H_{f,0}$ [22–24] of CH_3CH_2SH, H, and CH_3CH_2S for the channel of H abstraction from SH group. This value is in excellent agreement with the result calculated at the the QCISD(T)/6-311 + G(3df, 2p) level, especially if the experimental uncertainties are taken into consideration. Because of the absence of experiment standard heats of formation for other species, no available experimental reaction enthalpies were obtained for the channels of H abstraction from CH_3, CH_2 group and substitution channel. With respect to the barrier height, a direct comparison of theory with experiment is not possible. Taking into account the calculated result of the reaction enthalpy, we have chosen the potential barriers calculated at the QCISD(T)/6-311 + G(3df, 2p) level for the following kinetics calculations. At the QCISD(T)/6-311 + G(3df, 2p) theory level, the channel of H abstraction from SH group has the lowest potential barrier of 3.2 kcal/mol, which means that H abstraction from SH group will be dominant channel. The potential barriers of the channels of H abstraction from CH_3 and CH_2 groups is 5.9–10.7 kcal/mol higher than that of H abstraction from SH group. However, the barrier height of substitution channel is only 0.3 kcal/mol more than H abstraction from SH group. This means that substitution channel will be a strong competitive channel. This view is further testified by the following study of the rate constants and the branching ratios.

3.2. Kinetics calculation

3.2.1. Reaction path properties

With a step size of 0.05 $amu^{1/2}$ bohr, the intrinsic reaction coordinate (IRC) has been calculated at the MP2/6-

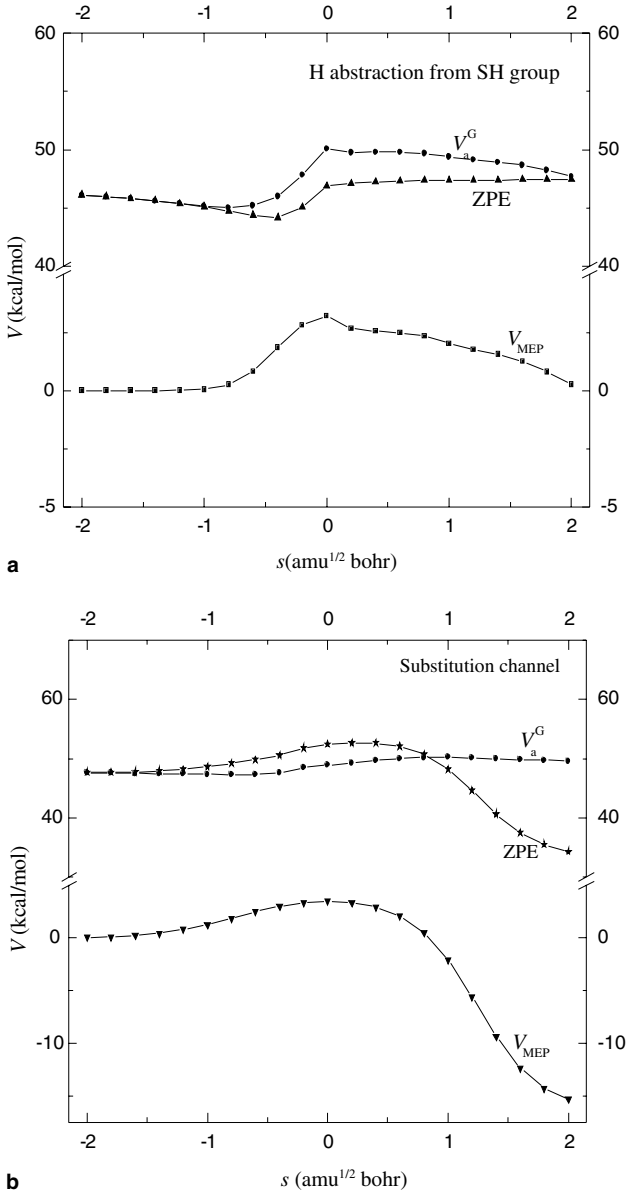

Fig. 3. (a,b) The classical potential energies (V_{MEP}), vibrationally adiabatic potential energies (V_a^G), and the zero-point energy (ZPE) curves as functions of s at the QCISD(T)/6-311+G(3df, 2p)//MP2/6-311G(2d, p) level for the channel of H abstraction from SH group and substitution channel.

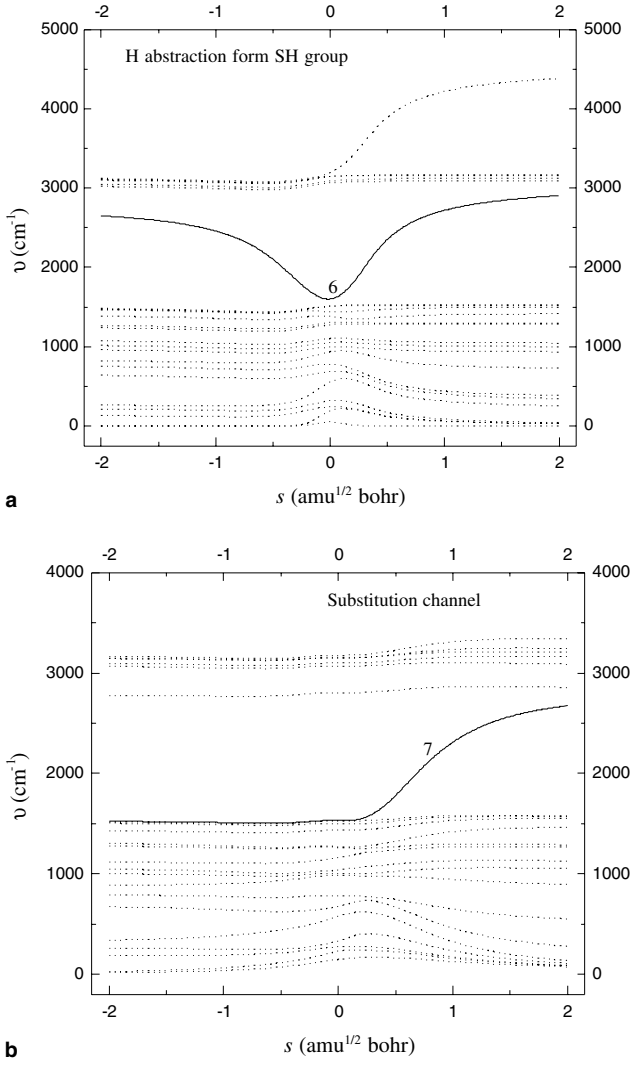

Fig. 4. (a,b) Changes of the generalized normal-mode vibrational frequencies as functions s at the MP2/6-311G(2d, p) level for the channel of H abstraction from SH group and substitution channel.

311G(2d, p) level from the saddle point to the reactants and the products for each channel. For substitution channel, the breaking S–C bond is almost unchanged from $s = -\infty$ to $s = -0.5\ \text{amu}^{1/2}$ bohr, equals the value in the reactant CH_3CH_2SH, and stretches almost linearly after $s = -0.5\ \text{amu}^{1/2}$ bohr. The forming S–H bond shortens rapidly from reactants and reaches the equilibrium bond length in H_2S at $s = 0.5\ \text{amu}^{1/2}$ bohr. Other bond lengths are almost unchanged during the reaction process. Therefore, the saddle point TS_4 connects the reactants (CH_3CH_2SH and H) with the products (CH_3CH_2 and H_2S). The geometric change mainly takes place in the region from $s = -0.5$ to $s = 0.5\ \text{amu}^{1/2}$ bohr. Similarly changes can be seen from abstraction channels.

The minimum energy path (MEP) for each reaction channel was obtained at the MP2/6-311G(2d, p) level by the IRC definition with a step size of $0.02\ \text{amu}^{1/2}$ bohr, and the energies of the MEP were refined by the QCISD(T)/6-311 + G(3df, 2p)//MP2/6-311G(2d, p) method. For all channels, the maximum position of the classical potential energy V_{MEP} curve at the QCISD(T)/6-311 + G(3df, 2p)//MP2/6-311G(2d, p) level corresponds to the saddle point structure at the MP2/6-311G(2d, p) level. Therefore, the shifting of the maximum position for the V_{MEP} curve caused by the computational technique is avoided (avoiding artificial variational effect) [25,26]. The classical potential energy V_{MEP}, the ground-state vibrational adiabatic potential energy V_a^G, and the zero-point energy (ZPE), where $V_a^G = V_{MEP} + \text{ZPE}$, as functions of the reaction coordinate s are plotted in Fig. 3(a) and (b)

Table 4
The CVT/SCT rate constants (in cm^3 $molecule^{-1}$ s^{-1}) along with the available experimental values [6,7] for all the channels involved in the reaction of CH_3CH_2SH with atomic H over the temperature range of 200–3000 K

T (K)	k_1	k_2	k_3	k_4	k	Expt.	Expt.
200	1.47E − 20	7.01E − 17	1.62E − 13	4.27E − 15	1.66E − 13		
250	1.31E − 19	3.20E − 16	4.38E − 13	2.10E − 14	4.59E − 13		
295	7.19E − 19	1.05E − 15	8.45E − 13	6.55E − 14	9.12E − 13		
298	7.28E − 19	1.13E − 15	8.75E − 13	6.98E − 14	9.46E − 13	1.25E − 12	2.4E − 12
300	8.10E − 19	1.19E − 15	9.00E − 13	7.31E − 14	9.74E − 13	1.27E − 12	
325	2.01E − 18	2.10E − 15	1.21E − 12	1.22E − 13	1.329E − 12	1.49E − 12	
350	5.11E − 18	3.53E − 15	1.56E − 12	1.93E − 13	1.76E − 12	1.72E − 12	
375	1.02E − 17	5.69E − 15	1.97E − 12	2.90E − 13	2.27E − 12	2.01E − 12	
400	2.00E − 17	8.79E − 15	2.44E − 12	4.18E − 13	2.86E − 12		
423	3.58E − 17	1.27E − 14	2.91E − 12	5.68E − 13	3.49E − 12	2.37E − 12	
450	6.81E − 17	1.91E − 14	3.52E − 12	7.80E − 13	4.32E − 12		
500	2.00E − 16	3.68E − 14	4.82E − 12	1.33E − 12	6.19E − 12		
600	1.18E − 15	1.09E − 13	8.10E − 12	3.05E − 12	1.13E − 11		
700	4.69E − 15	2.54E − 13	1.22E − 11	5.72E − 12	1.82E − 11		
800	1.42E − 14	5.10E − 13	1.73E − 11	9.44E − 12	2.72E − 11		
900	3.51E − 14	9.12E − 13	2.32E − 11	1.43E − 11	3.84E − 11		
1000	7.5E − 14	1.50E − 12	3.00E − 11	2.01E − 11	5.17E − 11		
1400	6.31E − 13	6.35E − 12	6.60E − 11	5.37E − 11	1.27E − 10		
1800	2.41E − 12	1.65E − 11	1.16E − 10	1.02E − 10	2.36E − 10		
2200	6.15E − 12	3.30E − 11	1.77E − 10	1.63E − 10	3.79E − 10		
2600	1.24E − 11	5.63E − 11	2.50E − 10	2.36E − 10	5.54E − 10		
3000	2.17E − 11	8.66E − 11	3.33E − 10	3.17E − 10	7.58E − 10		

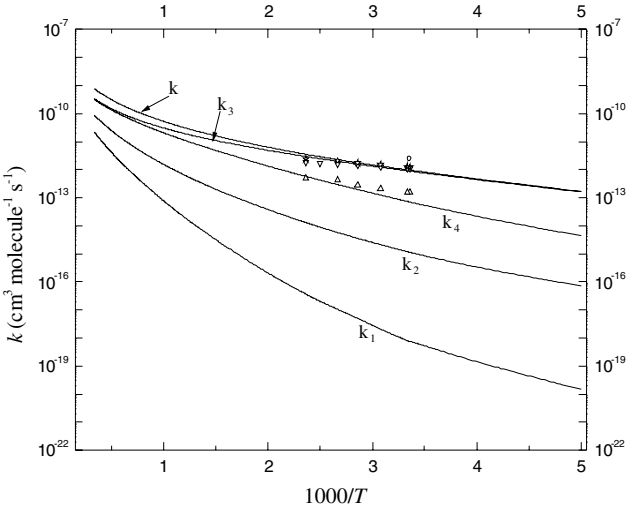

Fig. 5. CVT/SCT rate constants along with the experimental values [6,7] as function of the reciprocal of the temperature (T) over the temperature range of 200–3000 K. ▽, △ are the experimental rate constants of the channel of H abstraction from SH group and substitution channel, ○, ☆ are the experimental overall rate constants of the reaction of CH_3CH_2SH and atomic H.

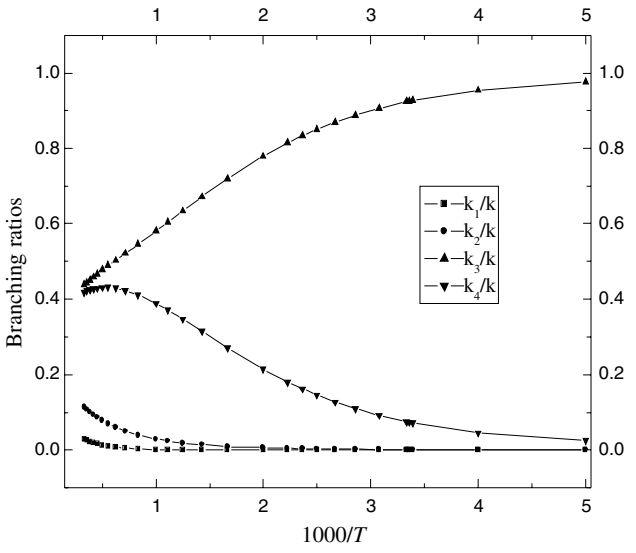

Fig. 6. The branching ratios as functions of the reciprocal of the temperature (T) over the temperature range of 200–3000 K.

for the channel of H abstraction from SH group and substitution channel. The V_{MEP} and V_a^G curves are similar in shape, and their maximum positions are almost the same. For the channel of H abstraction from SH group, the zero-point energy ZPE curve is nearly unchanged as s varies except that there is a gentle drop near the saddle point. Similarly changes can be seen from the channels of H abstraction from CH_3 and CH_2 groups. For substitution channel, the ZPE curve shows a slow increase from the reactants zone to the products zone. In order to analyze this behavior in greater detail, we show the variation of the generalized normal modes vibrational frequencies in Fig. 4(a) and (b) for the channel of H abstraction from SH group and substitution channel. Fig. 4(a) shows the vibrational mode 6 (reactive mode) drops dramatically near the saddle point for the channel of H abstraction from SH group. This behavior is known to be typical of hydrogen-transfer reactions [25–27]. This change causes a drop in

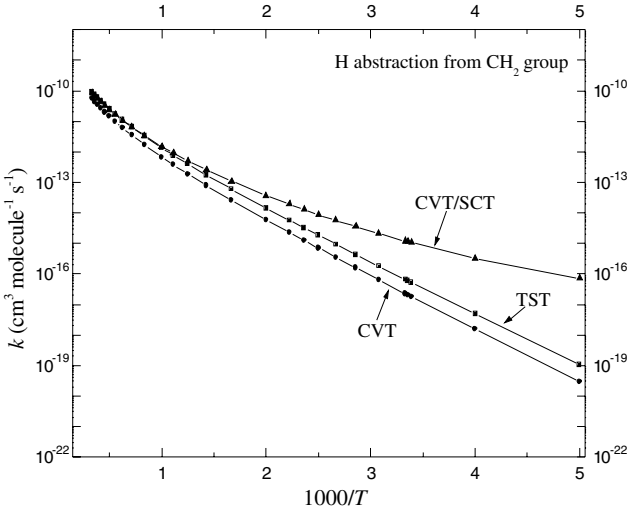

Fig. 7. TST, CVT, and CVT/SCT rate constants as function of the reciprocal of the temperature (T) over the temperature range of 200–3000 K for the channel of H abstraction from CH_2 group.

the ZPE curve. Similar behavior is also observed for the channels of H abstraction from CH_3 and CH_2 groups. For the substitution channel, the vibrational mode 7, which connects the frequency of C–S stretching vibration in CH_3CH_2SH with the frequency of the H–H stretching vibration of H_2, shows an obvious increase from the reactants zone to the products zone. This is in accordance with the change of the ZPE curve during the reaction process.

3.2.2. Rate constants

In this paper, the rate constants were calculated using the canonical variational transition-state theory (CVT) with a small curvature tunneling correction (SCT) contribution. This method has been successfully performed for several analogous reactions. For this multiple-channel reaction of CH_3CHSH with atomic H, the calculated CVT/SCT rate constants of H abstraction from CH_3, CH_2 and SH groups are denoted as k_1, k_2 and k_3, respectively, and the rate constants of substitution channel are denoted as k_4. It needs to be pointed that the rate constants k_1 are obtained as the sum of the calculated CVT/SCT rate constants of H abstraction from the C–H_a and C–H_b bonds in CH_3 group. The total rate constants of the reaction of CH_3CH_2SH with atomic H are noted as k, $k = k_1 + k_2 + k_3 + k_4$. The branching ratios are noted as k_1/k, k_2/k, k_3/k, and k_4/k, respectively. The calculated CVT/SCT rate constants and the branching ratios for all the channels along with the available experimental values are shown in Table 4 and Figs. 5 and 6. Several important features of the calculated rate constants are the following:

(1) Table 4 and Fig. 5 show that over the temperature range of 298–423 K, the total CVT/SCT rate constants, which is the sum of the CVT/SCT rate constants for all the channels, are in excellent with the available experimental values, with the maximum relative deviation less than 3 times. For example, at 298 K, The calculated total CVT/SCT rate constant is 9.46×10^{-13} cm^3 molecule^{-1} s^{-1}, which is in good agreement with the experimental values of 1.25×10^{-12} and 2.40×10^{-12} cm^3 molecule^{-1} s^{-1} [6,7]. Furthermore, the calculated CVT/SCT rate constants of the channel of H abstraction from SH group and substitution channel match the values obtained from the experimental Arrhenius expressions [7] reasonably well. Therefore, the CVT/SCT rate constants are taken as the accurate rate constants for each channel. Since there are no experimental data available at other temperatures except for the narrow temperature range 298–423 K, we hope our results may provide a good estimate for the kinetics of this reaction over a wide temperature range (200–3000 K).

(2) The branching ratios of each channel as functions of $1000/T$ are shown in Fig. 6. Due to having the smaller potential barrier, H abstraction from SH group is the fastest reaction channel, and CH_3CH_2S and H_2 are the dominant products. However, with the increase in temperature, substitution channel will be a strong competitive channel, especially when the temperature is higher than 1000 K. The contributions from the channels of H abstraction from CH_3 and CH_2 groups are minor at the lower temperature range. However, the rate constants of H abstraction from CH_3 and CH_2 groups increase rapidly with the increase in temperature. The k_1/k and k_2/k fractions are 1%, 8% at 2000 K, and 3% and 11% at 3000 K, respectively.

(3) For the purpose of comparison, the conventional transition-state theory (TST) rate constants and the variational transition-state theory (CVT) rate constants without the tunneling correction along with the CVT/SCT values are calculated. Fig. 7 shows the calculated TST, CVT and CVT/SCT rate constants for the channel of H abstraction from CH_2 group. At at 300 K, the CVT rate constant is 2.24×10^{-17} cm^3 molecule^{-1} s^{-1}, while the TST rate constant is 6.56×10^{-17} cm^3 molecule^{-1} s^{-1}. The latter is 2.9 times larger than the former. At 600, 1000, 1600 K, the TST rate constants are 2.3, 2.0 and 1.8 times larger than the CVT ones, respectively. In the temperature range of 200–1000 K, the CVT rate constants are much smaller than that of CVT/SCT. For example, at 298 K, the CVT rate constant is 2.04×10^{-17} cm^3 molecule^{-1} s^{-1}, while the CVT/SCT rate constant is 1.13×10^{-15} cm^3 molecule^{-1} s^{-1}. The latter is 55 times larger than the former. With the increase in temperature, the CVT/SCT rate constants are asymptotic to those of CVT. This means only in the lower temperature ranges does the small curvature tunneling correction play an important role for the calculation of the rate constants. The same conclusion can be drawn from other channels.

(3) The calculated rate constants exhibit typical non-*Arrhenius* behavior. This non-*Arrhenius* behavior has frequently been observed in radical–molecule reactions studied over wide temperature ranges [28]. The CVT/SCT rate constants of the title reaction are fitted by a three-parameter formula over the temperature range of 200–3000 K and given in units of cm^3 $molecule^{-1}$ s^{-1} as follows:

$$k_1 = 2.92 \times 10^{-27} T^{4.71} \exp(-2125.13/T);$$

$$k_2 = 6.57 \times 10^{-22} T^{3.28} \exp(-1244.6/T);$$

$$k_3 = 1.59 \times 10^{-16} T^{1.84} \exp(-561.3/T);$$

$$k_4 = 4.55 \times 10^{-16} T^{1.75} \exp(-1448.0/T);$$

$$k = 2.68 \times 10^{-17} T^{2.17} \exp(-565.1/T).$$

(4) The Arrhenius form of the total CVT/SCT rate constants are fitted over the different temperature ranges and given in units of cm^3 $molecule^{-1}$ s^{-1} as follows:

$$k = 3.33 \times 10^{-11} \exp(-1063.1/T);$$

$$k = 7.15 \times 10^{-11} \exp(-1292.6/T);$$

$$k = 3.17 \times 10^{-9} \exp(-4680.6/T).$$

It can be seen that the Arrhenius activation energy increases with the increase in temperature [28].

4. Conclusion

In this paper, we present an exhaustive and theoretical study on the multiple-channel reaction of CH_3CH_2SH with atomic H using ab initio direct dynamics method. Five saddle points, which correspond to two different reactive sites in CH_3CH_2SH, were located. The comprehensive dynamics study on all the channels using canonical variational transition-state theory (CVT) with small-curvature tunneling effect has led to the following specific conclusions:

(1) Over the temperature range of 298–423 K, the CVT/SCT overall rate constants are in good agreement with the available experimental values.
(2) The channel of H abstraction from SH group is dominant channel. However, as the temperature increases, substitution channel becomes a strong competitive channel.
(3) The variational effect is small for all the channels.
(4) The small curvature tunneling correction plays an important role for the calculation of the rate constants.

Acknowledgements

The authors thank Professor Donald G. Truhlar for providing the POLYRATE 9.3 program. This work is supported by Program for New Century Excellent Talents in University (NCET-04-036).

References

[1] G.S. Tyndall, A.R. Ravishankara, Int. J. Chem. Kinet. 23 (1991) 483.
[2] J.N. Galloway, Water Air Soil Pollut. 130 (2001) 17.
[3] M.O. Andreae, H. Raemdonck, Science 221 (1983) 744.
[4] B.F. Taylor, R.P. Kiene, in: E.S. Saltzman, W.J. Cooper (Eds.), Biogenic Sulfur in the Environment, ACS Symposium Series, vol. 393, American Chemical Society, Washington, 1989, p. 202.
[5] R.R. Kuntz, J. Phys. Chem. 71 (1967) 3343.
[6] D. Martin, J.L. Jourdain, G. Le Bras, Int. J. Chem. Kinet. 20 (1988) 897.
[7] W.W. Lam, T. Yokota, I. Safarik, O.P. Strausz, J. Photochem. Photobiol. A 47 (1989) 47.
[8] A. Gonzalez-Lafont, T.N. Truong, D.G. Truhlar, J. Chem. Phys. 95 (1991) 8875.
[9] B.C. Garrett, D.G. Truhlar, J. Phys. Chem. 83 (1979) 1052.
[10] B.C. Garrett, D.G. Truhlar, R.S. Grev, A.W. Magnuson, J. Phys. Chem. 84 (1980) 1730.
[11] D.G. Truhlar, A.D. Isaacson, B.C. Garrett, in: M. Baer (Ed.), Generalized Transition State Theory, vol. 4, CRC Press, Boca Raton, FL, 1985, p. 65.
[12] Y.-P. Liu, G.C. Lynch, T.N. Truong, D.-H. Lu, D.G. Truhlar, B.C. Garrett, J. Am. Chem. Soc. 115 (1993) 2408.
[13] M.J. Frisch, G.W. Trucks, H.B. Schlegel, P.W.M. Gill, B.G. Johnson, M.A. Robb, J.R. Cheeseman, T.A. Keith, G.A. Petersson, J.A. Montgomery, K. Raghavachari, M.A. Allaham, V.G. Zakrzewski, J.V. Ortiz, J.B. Foresman, J. Cioslowski, B.B. Stefanov, A. Nanayakkara, M. Challacombe, C.Y. Peng, P.Y. Ayala, W. Chen, M.W. Wong, J.L. Andres, E.S. Replogle, R. Gomperts, R.L. Martin, D.J. Fox, J.S. Binkley, D.J. Defrees, J. Baker, J.P. Stewart, M. Head-Gordon, C. Gonzales, J.A. Pople, Gaussian03, Pittsburgh, PA, 2003.
[14] B.C. Garett, D.G. Truhlar, J. Phys. Chem. 87 (1983) 4553.
[15] R. Steckler, Y.Y. Chuang, P.L. Fast, J.C. Corchade, E.L. Coitino, W.P. Hu, G.C. Lynch, K. Nguyen, C.F. Jackells, M.Z. Gu, I. Rossi, S. Clayton, V. Melissas, B.C. Garrett, A.D. Isaacson, D.G. Truhlar, POLYRATE Version7.8, University of Minnesota, Minneapolis, 2003.
[16] Kuchitsu (Ed.), Landolt–Bornstein: Group II: Atomic and Molecular Physics, Structure Data of Free Polyatomic Molecules, vol. 15, Springer-Verlag, Berlin, 1987.
[17] G. Herzberg, Electronic Spectra and Electronic Structure of Polyatomic Molecules, Van Nostrand, New York, 1966.
[18] L.M. Sverdlov, M.A. Kovner, E.P. Krainov, Vibrational Spectra of Polyatomic Molecules, Wiley, New York, 1974.
[19] M.E. Jacox, Vibrational and electronic energy levels of polyatomic transient molecules, J. Phys. Chem. Ref. Data Monogr. 3 (1994) (updated data in NIST Chemistry Webbook).
[20] T. Shimanouchi, Tables of Molecular Vibrational Frequencies, Consolidated Volume 1, NSRDS NBS-39.
[21] G.S. Hammmond, J. Am. Chem. Soc. 77 (1955) 334.
[22] M. Frenkel, K.N. Marsh, R.C. Wilhoit, G.J. Kabo, G.N. Roganov, Thermodynamics of Organic Compounds in the Gas State, Thermodynamics Research Center, College Station, TX, 1994.
[23] L.V. Gurvich, I.V. Veyts, C.B. Alcock, Thermodynamic Properties of Individual Substances, 4th ed., Hemisphere Pub. Co., New York, 1989.
[24] J.D. Cox, D.D. Wagman, V.A. Medvedev, CODATA Key Values for Thermodynamics, Hemisphere, New York, 1989.
[25] J. Espinosa-Garcia, J.C. Corchado, J. Phys. Chem 100 (1996) 16561.
[26] J.C. Corchado, J. Espinosa-Garcia, J. Chem. Phys. 106 (1997) 4013.
[27] J. Espinosa-Garcia, J.C. Corchado, J. Phys. Chem. 101 (1997) 7336.
[28] B.C. Garrett, D.G. Truhlar, J.M. Bowman, A.F. Wagner, D. Robie, S. Arepalli, N. Presser, R.J. Gordon, J. Am. Chem. Soc. 108 (1986) 3515.